Modeling, Development and Control of Linear Twisted-String Actuator

Djordje Urukalo, Milos D Jovanovic, Aleksandar Rodic

Mihailo Pupin Institute, Volgina 15, 11000 Belgrade, Serbia
djordje.urukalo@pupin.rs, milos.jovanovic@pupin.rs, aleksandar.rodic@pupin.rs

Abstract: For the scientific community worldwide, developing a new actuator is a challenging task. New types of actuators are needed, especially in humanoid robotics in order to replace real human muscle. There are several approaches for how to obtain this goal. One approach is to realize real muscle using new synthetic materials such as piezoelectric components or pneumatic polymer materials. A second approach is to improve standard electromotor-gear actuators. Another unconventional approach is to use standard electromotor together with a tendon-based driving system. This paper presents a successful realization and control model for a proposed twisted-string actuator. Controller design is based on the National Instruments Single Board RIO driving a MAXON motor type tendon driven muscle. A Powerful Spartan FPGA is a key element for the presented hardware implementation. To program the whole system, LabVIEW software is used. Theoretically explained simulation results for adopted model design, as well as real measured experimental movement under the load force, are presented in the paper.

Keywords: twisted string; tendon; actuator; SB-Rio; LabVIEW

1 Introduction

Bio-inspired humanoid robotics and its realization is currently a promising area of research activity. One of the main goals today in the scientific community and technology is the realization of an efficient electrically-driven actuator that is comparable with real human muscle. The musculoskeletal system of the human body is one of the most well-known sophisticated actuation systems worldwide. Since nature took thousands of years to optimize each particular muscle of the human body, it is then obvious that biological knowledge of the human body should be taken into account in order to design a bio-inspired artificial muscle. Several different types of criteria must be satisfied: approx. same mass and dimensions of the artificial muscle and the human body muscle, maximum payload fraction, satisfactory speed and payload, precision and repeatability in a range of human skill, linear actuation in order to imitate biological muscle, compliancy actuation, etc. Recently, a lot of work has been carried out in order to

create artificial muscle (Figure 1) that is similar to the characteristics of human muscle, such as: pneumatic McKibben actuator [1], electroactive polymer actuators as artificial muscles [2], piezoelectric muscle-like actuator [3], shape memory alloys [4] and many other technical solutions.

Figure 1

The world realized artificial muscle: McKibben [1] pneumatic actuator (top-left), electroactive polymer actuators [2] (top-right), shape memory alloys [4] (down-left), piezoelectric muscle-like actuator (down-right) [3]

Numerous authors have already presented technical realizations of human-like actuation in robotics, such as: tendon driven antagonistic robotic actuator at the German Aerospace Center (DLR) [5], antagonistically coupled pneumatic actuator at Osaka University [6], and the Japanese robot Kenshiro from University of Tokyo [7].

Pneumatic actuators deal with high forces and displacement, however, distribution of control signals takes a huge amount of space. They are noisy and have a significant hysteresis work ratio. Electroactive polymer actuators sustain large forces for a small displacement. A large activation voltage is necessary for these types of actuators. Shape memory alloy actuators have high energy density, easy control, compact, and good mechanical properties, but they are rather expensive and they have a slow dynamic response and poor fatigue properties. Piezoelectric muscle-like actuators are suited only for very small forces and displacements. It is extremely difficult to control such kinds of devices because of problems with a very high hysteresis and memory effect.

Another proposed approach is from researchers at Duke University in Durham, USA; they revealed that they have grown the first ever human skeletal muscle that contracts in response to external stimuli, such as electrical impulses and pharmaceuticals [8]. This is a very promising area of research because it is obvious that natural muscle is the best possible actuator regarding the power efficiency versus realized force and torque, especially when compared to some other mechanical drive systems. If it will be possible to implement such kinds of

laboratory grown muscles to mechanical systems, extreme technical improvement needs to be done regarding the realized force and torque, high dynamic of the systems and even full system control. Of course, a lot of obstacles should be solved, such as a mechanical connection between human tissue and the external links and especially the problem of how to "power" such kinds of hybrid systems Some kind of bio power circulation for tissue should be realized to preserve the functionality and lifetime of the laboratory grown muscle.

In this paper, a twisted-string linear actuator is realized and presented in the paper as a light-weight, low-noise and compact linear design with high-speed actuation and satisfactory high payload.

2   Problem Statements and Task Description

A linear twisted-string actuator is designed to produce movement in a humanoid robot arm that is close to the movement of a human arm with similar requirements of speed and force. By taking into account the human arm dimension and natural human arm movement, artificial muscle requirements are calculated and simulated.

In order to estimate the required shoulder arm torque and composite speed at the end of the hand for natural human arm movement, a simulation of 7 degrees of freedom (d.o.f.) robotic arm in MATLAB is carried out [9-11]. Robotic arm parameters in standard D-H notation as well as masses of the segments used in the simulation are listed in the Table 1.

Table 1
Required robotic arm parameters and segment mass

Link i	a_{i-1}	α_{i-1}	d_i	Θ_i	m [kg]
1	0	$-\pi/2$	0	0	0
2	0	$-\pi/2$	0	0	0.223
3	-0.3	0	0	0	2.276
4	0	$\pi/2$	0	0	0.795
5	0	$-\pi/2$	0.3	0	0.586
6	0	$-\pi/2$	0	0	0.059
Tool	0.22	$\pi/2$	0	$-\pi$	0.213

The circular movement of the robotic arm by carrying the load of 1 kg for 6.5 seconds in the frontal plane is simulated. Mass hand center trajectory for this movement is shown on Figure 2:
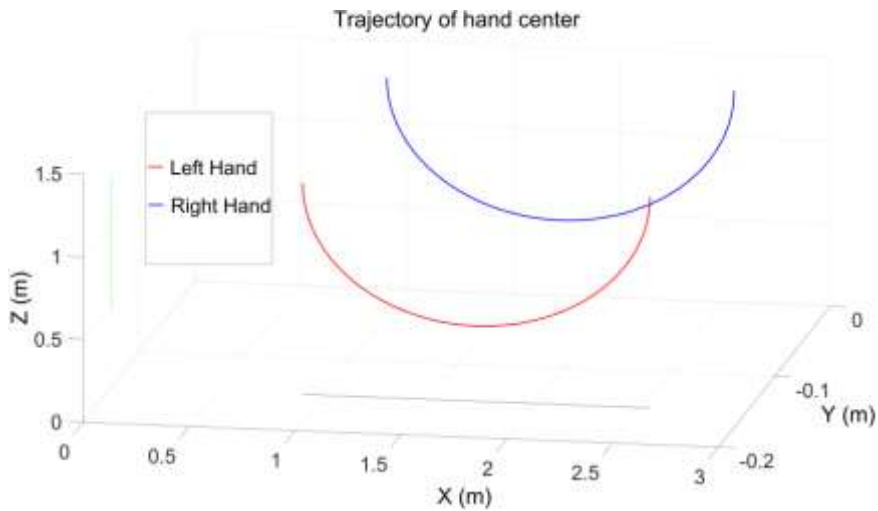
Figure 2

Mass hand center trajectory for circular movement of arms carrying 1 kg load. Duration of the movement is 6.5s.

Hand velocity v_{HAND} and acceleration a_{HAND} are calculated by using the following equations:

$$v_{HAND} = J_{HAND}\dot{Q} \tag{1}$$

$$a_{HAND} = J_{HAND}\ddot{Q} + \ddot{J}_{HAND}Q^2 \tag{2}$$

Where J_{HAND} is Jacobian matrix.

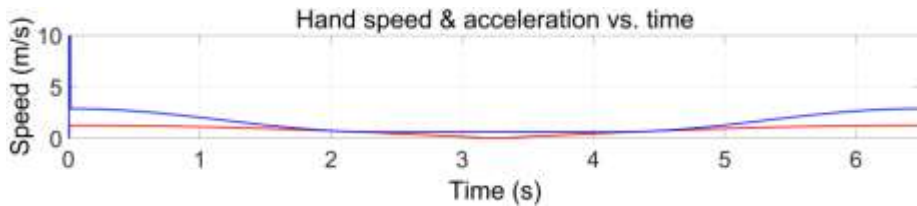During the simulation, a maximum composite speed of 3 m/s at the center of the hand is found (Figure 3).

Figure 3

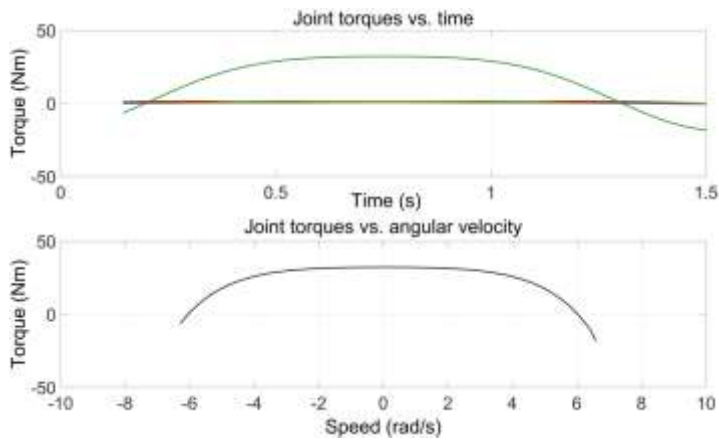Calculated hand speed and acceleration in time

Figure 4

Joint torques versus time and angular velocity

Required shoulder arm torque (Figure 4) of maximum 20.89 Nm as well as other joint torques is determined using inverse dynamics from the simulation accordingly:

$$\tau = H(Q)\ddot{Q} + C(Q,\dot{Q})\dot{Q} + G(Q) - J_{HAND}{}^{T}F \tag{3}$$

Q, $\dot{Q}$, $\ddot{Q}$ are the vectors of generalized joint coordinates, velocities, and accelerations. H is the joint-space inertia matrix, C is the Coriolis and a centripetal coupling matrix, F is the friction force, and G is the gravity loading. The last term gives the joint forces due to a wrench F that is applied to the end effector.
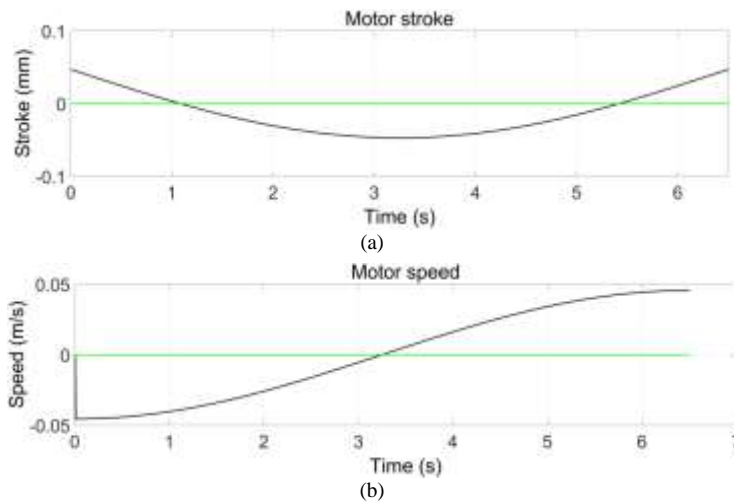

Figure 5

Calculated motor speed (a) and stroke (b) for linear actuator

Actuator linear motion in pulling direction of maximum 0.05 m is calculated as Motor stroke L_{MOTOR} accordingly (Figure 5a):

$$L_{MOTOR} = r_{MOTOR}(Q - Q_0) \tag{4}$$

Actuator pulling speed of maximum 0.05 m/s is determined as linear motor speed v_{MOTOR} (Figure 5b) accordingly:

$$v_{MOTOR} = r_{MOTOR}\dot{Q} \tag{5}$$

Actuator pulling force up to 696.2 N is found as the total tensile motor force for a certain degree of freedom, F_{MOTOR} (Figure 6), which is calculated by using the following equation:

$$F_{MOTOR} = \frac{\tau_{MOTOR}}{r_{MOTOR}} \tag{6}$$

Figure 6

Calculated motor payload for linear actuator

for which r_{MOTOR} represents the winch radius and Q_0 is zero position.

Figure 7

Design of proposed linear twisted-string acutator: 1. DC motor, 2. Gearhead, 3. Coupling, 4. Bearing, 5. Spring holder, 6. Spring, 7. Twisted-string, 8. Tube, 9. Driving part, 10. Bracket

To satisfy previously explained requirements, new approaches in mechanics should be introduced. For this purpose, the authors proposed a rather new design, twisted-string linear actuator (Figure 7), which has a tube structure with light-weight, low-noise, and compact linear design with high-speed actuation and satisfactory payload value.

This type of actuator should be used for driving humanoid robotic arms and hands. It is planned to use four twisted-string artificial muscles to actuate a humanoid arm without a hand in the following order: shoulder pitch and roll, elbow pitch, lower arm yaw (Figure 8). Actuators for shoulder pitch and roll joints will be placed inside the torso of a humanoid robot, and other two actuators will be placed in the upper arm link.
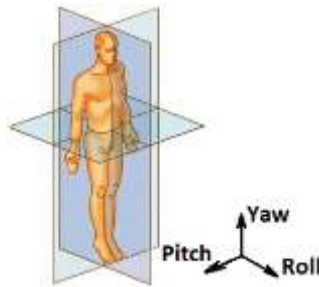

Figure 8
Possible angle of rotation of human's body [12]

Movement of a humanoid robotic hand will be realized with several twisted-string artificial muscles placed circularly in the lower-arm link. The total number for activating a robotic hand is still under investigation. Complex mechanical design as well as control of a light-weight humanoid robotic arm will be the next challengeable task in the future. This is still a promising new approach because of its complexity. There are some works concerning activation of only elbow joints with this type of actuator [13]. Here it is presented as a mechatronic design and experimental evaluation of synergy-based control for human-like grasping of robotic hand within the Dexmart Project [9, 12]. Several StMA-based hexapod walking robots are presented to the public [14].

3   Mechanical Design

Our proposed and realized twisted-string actuator is composed of one Maxon DC motor (20 W) (Figure 9, part 1) [15] that is equipped with an incremental optical encoder CPT1000 [17] and a planetary gearhead that has a ratio of 19.2:1 (Figure 9, part 2) [16]. Other mechanical parts of twisted-string actuators are: axial bearing FAG 51100 (Figure 9, part 3) [18], spring (Figure 9, part 4), coupling (Figure 9, part 5), 4 linear guides (Figure 9, part 6) with appropriate linear bearings (Figure 9, part 7), two brackets (Figure 9, part 8 and part 9), strings (Falcon Fishing Tackle, Catfish Leader, 146 kg) (Figure 9, part 10) and the stand (Figure 9, part 11). Other parts are not labeled. Complete mechanical design is presented in the Figure 9.
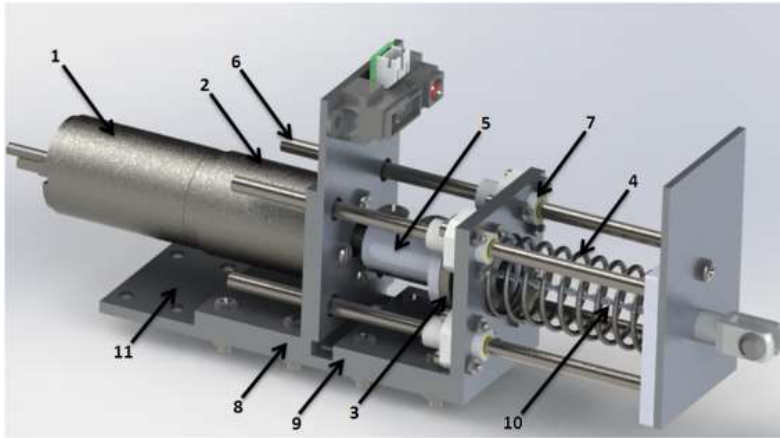
Figure 9

Mechanical design of twisted-string actuator with separate mechanical parts (1-DC motor with encoder; 2-planetary gearhead; 3-axial bearing; 4-spring; 5-coupling; 6-linear guides; 7-linear bearing; 8, 9-brackets; 10-string; 11-stand

DC motor with a gearhead is connected to the bracket, and the bracket is connected to the stand. An incremental encoder is used for actuator movement control. Another bracket is used for supporting 4 linear bearings that serve to lead 4 guides of 4mm diameter each in linear parallel motion. This bracket is also used to support the axial bearing that prevents gearhead from destruction of carrying a high axial load by twisting 4 non-tensile and high-flexible strings of 1mm diameter each. A spring is used for turning the actuator back to the initial position of maximum actuator displacement. The spring should be well-chosen; it should be powerful enough to overcome friction losses between linear bearings and guides, as well as friction losses inside twisted strings. If the actuator is mounted only in a vertical position, lifting and lowering the load, the spring is not necessary and could be removed from an actuator.

4   Controller Design

Global block diagram control scheme is shown on Figure 10. Standard PC computer is connected with Escon motor driver module [19] via USB in order to tune the current and the speed control loop; it is also used for monitoring controller's states and the DC motor's states with LabVIEW [20]. Escon module is in fact a smart DC motor driver. It consists one MOSFET H bridge together with an intelligent controller that is capable of realizing speed, current, and velocity control of the DC motor in the loop.
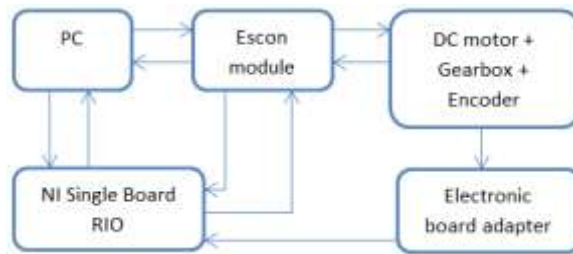
Figure 10
Global block diagram of controller design of twisted-string actuator

A PC computer is also connected to an NI Single-Board RIO 9636 [21] using ethernet cable in order to establish data acquisition of the measured signals in the system by LabWIEW. NI SbRIO 9636 is a powerful ARM based microcontroller board that operates under the real time NI OS. It consists of a 400 MHz ARM microcontroller and powerful SPARTAN FPGA running up to 40MHz. It has 48 programmable digital and analog IO pins which could be directly controlled by the FPGA or ARM microcontroller. Some IO pins could be both analog and digital according to the users.

A special electronic adapter board is realized to obtain 16-bit counter data which is received from the differential line encoder and filtered with high-speed logic circuits. NI Single-Board RIO is also connected to the ESCON module by some separate digital lines. Through this connection, the NI board can set motor current, speed, and direction of motor rotation acquiring the encoder's data in time during the movement. The Escon module also has the information about the encoder's data during the movement of the motor.
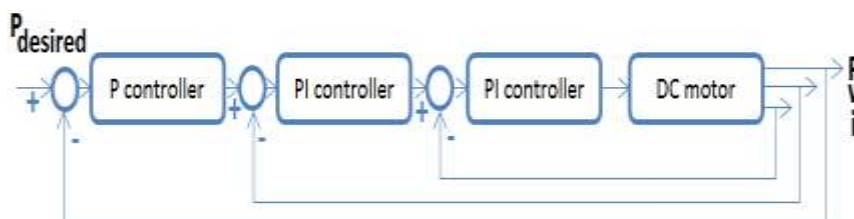

Figure 11
Cascade control structure for actuator control

A unique cascade control scheme (Figure 11) is realized to establish position and velocity control of a DC motor [22] and the whole actuator. Flexibility is a key feature of this type of controller. It consists of three distinct control loops: the innermost current loop is followed by the speed loop, and the speed loop is followed by an outermost position loop. This type of control requires increasing the response time of the controller towards the inner loop. In other words, the current loop is the fastest and the position loop is the slowest.

5   Model Analysis and Simulation Results

In order to control a twisted-string actuator, it is necessary to find a correct mathematical model that describes real physical systems. Until now, different analyses of twisted-string actuators have been carried out. Helix schematic representations of twisted-strings are used in modeling load position p (Figure 12).
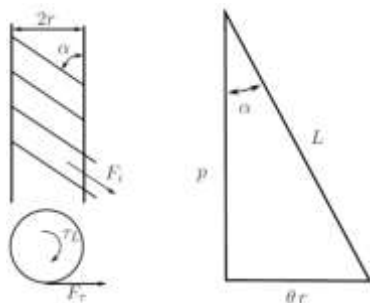

Figure 12

Helix schematic representation of twisted string

The parameters for modeling twisted-string actuators are: L-string length, θ-twisting angle, r-radius, α-helix slope, F_i -axial force of each string, τ_L-external torque, and F_τ -the tangential force. Position p is expressed by simple equations applying Pythagoras's theorem [23], where fiber tension is taken into account as well as stiffness, actuator rotation, and the radius of the string. Variations of the twisted-string radius with the twisting angle are included in [13]. The final model after consideration of the effective length of twisted string as a function of the number of turns is given in [24]. One simple model of load position is given in [9, 25-26]. Since proposed models of load position *p* mismatch measured load positions in real experiments, load position is expressed as a function of motor position (θ_M) and load (F_L) (7). Minimization processes between measured ($p_i^{measured}$) and obtained ($p_i^{obtained}$) load positions are taken into account by (8). It is done using the LM algorithm [27-28].

$$p_i^{obtained} = c_1 + c_2\theta_M + c_3\theta_M^2 + c_4F_L \tag{7}$$

$$\min_{\theta_M,F_L} f(\theta_M, F_L) = \|F(\theta_M, F_L)\|_2^2 = \sum_i F_i^2(\theta_M, F_L) = \sum_i \left(p_i^{measured} - p_i^{obtained}\right)^2 \tag{8}$$

Minimization converged and residual is $1.0077 \cdot 10^{-5}$. The coefficients of the equation (7) are listed in the Table 2 and they are calculated using the simulation.

Table 2

Required robotic arm parameters and segment mass

c_1	0.0897
c_2	4.7922e-06
c_3	-9.5170e-09
c_4	3.2083e-05

Unloaded and untwisted string length L_0 is estimated (coefficient c_1 in equation (7)) and it will be used hereafter. Figure 13 represents lengths of twisted strings as a function of load and motor position. The points represent measured lengths of twisted-strings, and lines represent obtained lengths of twisted strings used (7).
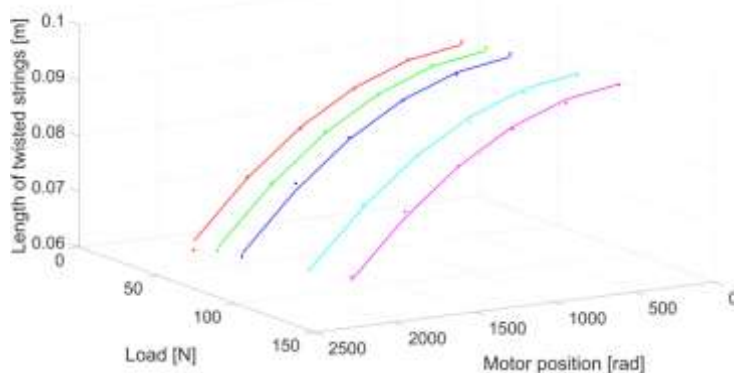

Figure 13
Lengths of twisted strings: measured points $\boldsymbol{p}_i^{measured}$ and obtained points $\boldsymbol{p}_i^{obtained}$

Hence, it is not possible to have a 100% malleable string, obtained load position is found applying Pythagoras's theorem (Figure 12), where ΔL is string elongation (9). String elongation is expressed as a function of motor position and load (10). Estimated unloaded and untwisted string's length $L_0 = 0.0897m$ is taken from Table 3. In order to find coefficients for equation (10) (listed in Table 3), a minimization process between measured $p_i^{measured}$ and obtained $p_i^{obtained}$ load positions are carried out (11).

$$p_i^{obtained} = \sqrt{(L_0 + \Delta L)^2 - (\theta_M r)^2} \qquad (9)$$

$$\Delta L = f(\theta_M, F_L) = a_1 \theta_M + a_2 \theta_M^2 + a_3 F_L \qquad (10)$$

$$\Sigma_i \left(p_i^{measured} - p_i^{obtained} \right)^2 \qquad (11)$$

Table 3
Coefficients of equation (10)

a_1	8.1153e-06
a_2	8.4427e-09
a_3	1.6914e-05

Residual of minimization function (11) is $1.1403 \cdot 10^{-5}$.

Motor torque is estimated using the same principle as described earlier. The axial force of each string F_i can be found using Pythagoras's theorem (12):

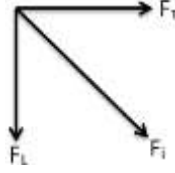$$F_i = \sqrt{F_L^2 + F_\tau^2} \qquad (12)$$

Figure 14

Decomposition of axial force of each string

Calculated axial force (12) in string F_I as a function of load and motor position is shown on Figure 14.

Transmission ratio can be found using:

$$\frac{\tau_L}{F_L} = \frac{\theta r^2}{p} \tag{13}$$

The tangential force F_τ (15) can be found transferring equation (13) and taking into account:

$$\tau_L = F_\tau r \tag{14}$$

$$F_\tau = \frac{F_L \theta_M r}{p} \tag{15}$$

Calculated motor torque (16) is ratio of gear torque τ_G and gear ratio i, where previous equations are used.

$$\tau_{M_i}^{calculated} = \frac{\tau_G}{i} = \frac{F_L \theta_G r^2}{i p_i^{measured}} = \frac{F_L r^2 \theta_M}{i^2 p_i^{measured}} \tag{16}$$

Obtained motor torque is expressed as the following:

$$\tau_{M_i}^{obtained} = b_1 + b_2 \theta_M + b_3 \theta_M^2 + b_4 F_L + b_5 F_L \theta_M \tag{17}$$

After the according minimization process:

$$\sum_i \left(\tau_{M_i}^{calculated} - \tau_{M_i}^{obtained} \right)^2 \tag{18}$$

Coefficients b_1 to b_5 are obtained and presented in Table 4, where the residual is $1.7743 \cdot 10^{-6}$.

Table 4

Obtained motor torque coefficients

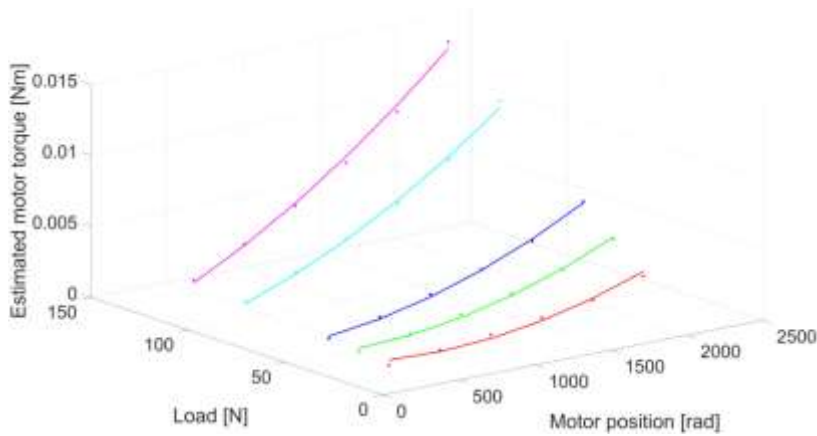|	
b_1	0.0014
b_2	-3.1935e
b_3	1.4529e-09
b_4	-1.2142e-05
b_5	6.0940e-08

Figure 15
Estimated motor torque as a function of load and motor position

Motor position and motor load position dependency of calculated and estimated motor torque are shown on Figure 15.
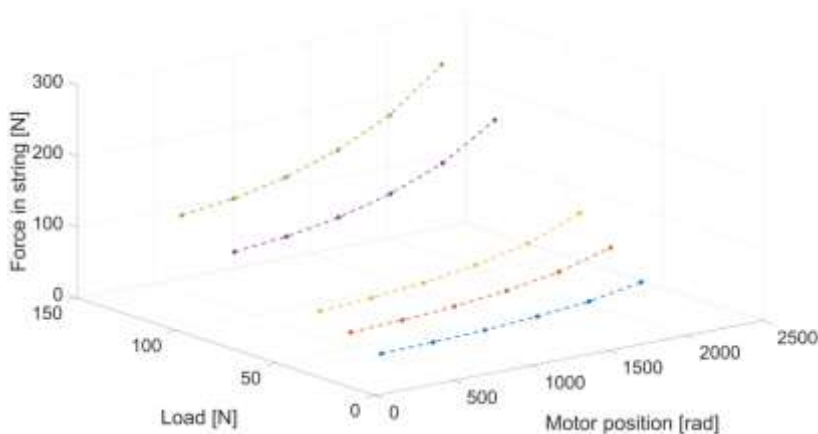

Figure 16
Estimated axial force in string as a function of load and motor position

Figure 16 presents dependency of calculated and estimated string force in relation to motor position and motor load.

Helix slope α is calculated using the following equation:

$$\alpha = \text{acos}(\frac{F_L}{nF_i}) \tag{19}$$

Where n is the number of strings, which is 4 in the presented experiment. A relationship of Helix slope as a function of load and motor position is represented in Figure 17.

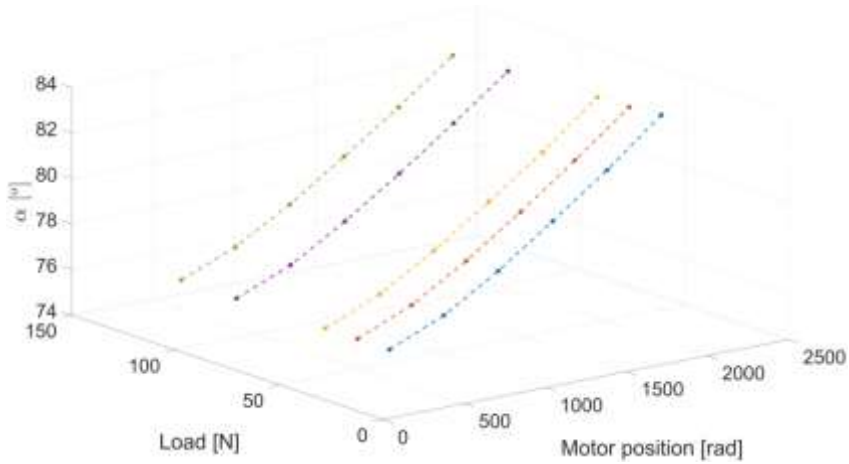A small variation of angle α will produce a large load position p-variation.

Figure 17

Helix slope as a function of load and motor position

6   Experimental Results

As mentioned before, a linear twisted-string actuator is placed in a vertical position. Different loads are applied onto the actuator in order to replicate weights of human muscle's load realistically. The loads of 23 N, 39 N, 54 N, 97 N and 124 N are applied. Strings are terminated on aluminum plates with 4 holes and twisted with the actuator from 0 to 7000 degrees with a step of 1000 degrees. A set of points from real experiment are obtained and presented onto the diagrams (Figure 13. Figure 15 and Figure 18). In Figure 18 a relationship between string length as a function of actuator rotation for each load is depicted.

There are quadratic regressions in a range from 0-6000 degrees of rotation angle where strings behave regularly, i.e. strings twist till maximum possible angle - strings pack properly. Above 6000 degrees of rotation angle, non-regular strings packaging appear. In such a way, several stress concentrations can cause strings to break.
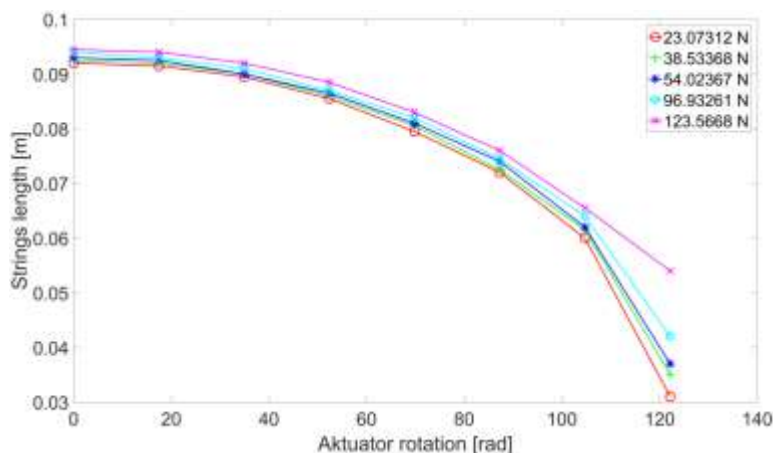
Figure 18

String's length as a function of actuator rotation

The speed and current control loops are tuned to the ESCON auto tuning process using required ESCON control software. The *P* gain of the position controller is found manually. Controller's parameters are listed in the Table 5.

Table 5

Applicated controller gains for a DC motor during the test

Controller	P gain	Integration time constant
Position	0.0035	-
Speed	963	42ms
Current	165	69μs

Maintaining stable control of a DC motor with maximum steady-state position error of 2 degrees is realized with hysteresis. An error of 2 degrees in position suits the presented application since the motor rotation is in thousands of degrees with four times multiplying encoding of optical differential encoder of 1000 CPT and the planetary gearbox with ratio 19.2:1. Stabilization of the motor position in hysteresis control is done by using a huge first order RC circuit with a time constant of 1^{10} seconds where states (20-21):

$$PV > SP - 2° \tag{20}$$

$$PV < SP + 2° \tag{21}$$

Where PV is Process Variable and SP is Set Point.

The main objective of this work is to make an actuator with similar characteristics of real human muscle. One of the characteristics of real human muscle is stiffness. Artificial twisted-string actuator has a property of stiffness that varies with motor position (Figure 19). That will give compliance in actuation of humanoid robotic arm.
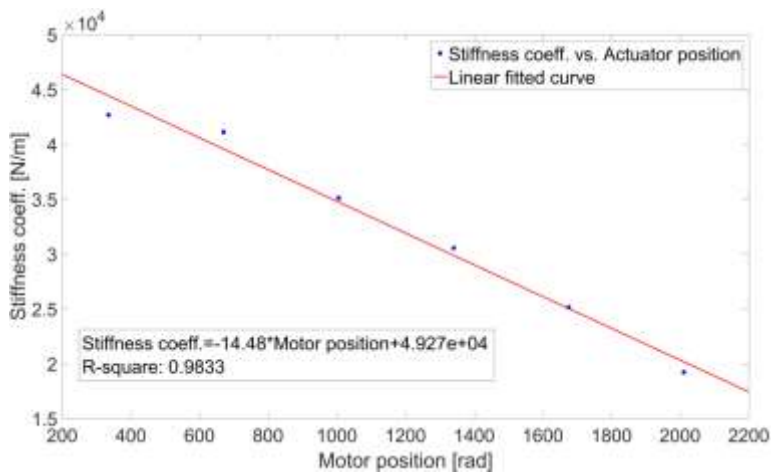
Figure 19
Stiffness coefficient as a function of motor position

Each point is obtained from a linear regression model of load versus string's length where correlation coefficients are: 0.9617, 0.9655, 0.9323, 0.9723, 0.9290, and 0.9855. It has to be noted that the first and last points are excluded to achieve a linear dependency role in decreasing manner of the twisted-strings stiffness coefficient versus actuator rotation with satisfied correlation coefficient of 0.9833.

For motor range between {335.1 – 2011} rad, string's length changes in range of {0.0315; 0.0305; 0.0305; 0.0290; 0.0285;} m, and considering a maximum rotation speed of 8000RPM is limited to a maximum permissible input speed in gearhead and maximum measured actuator speeds are successfully {1.58; 1.53; 1.53; 1.45; 1.42} cm/sec.

Conclusions

In the paper a new proposed twisted-string linear actuator is designed and realized (Figure 20). Characteristics of twisted-strings artificial muscle are found and explained. Hardware and software control design are done and described in this work. The actuator is placed in a vertical position for lifting and lowering different loads. According to presented tasks, a robust and reliable control design is accomplished.

The presented realized design and proposed control algorithm of twisted-string actuator supports current intentions for realizing artificial muscle that is very close to the characteristics of the human arm muscle. Non-linear dependency model of the actuator is observed and explained. Twisted-string actuator has the characteristic of compliance similar to that of true human muscle. Compliance is followed with a stiffness that varies depending on actuator length in a linear descending manner. There is a limitation of speed and velocity of presented twisted string actuator compared to that of human muscle.

Figure 20
Pictures of realized and tested twisted-string actuator

Certainly more attention should be paid to string choice and termination in order to have reliable and long-term activation of a humanoid robot arm. Further dynamic analysis and dynamic characteristics should be done, as well as real implementation in a robotic arm.

Acknowledgement

References

[1]   F. Daerden, D. Lefeber, "Pneumatic Artificial Muscles: Actuators for Robotics and Automation", *European Journal of Mechanical and Environmental Engineering,* Vol. 47, pp. 10-21, 2000

[2]   Y. Bar-Cohen, *Electroactive Polymer (EAP) Actuators as Artificial Muscles: Reality, Potential, and Challenges,* 2nd ed., SPIE Press, Vol. PM136, 2004

[3]   T. Secord, "Design and Application of a Cellular, Piezoelectric, Artificial Muscle Actuator for Biorobotic Systems" Ph.D. dissertation, Dept. of Mechanical Engineering, Massachusetts Institute of Technology, Boston, Massachusetts, USA, 2010

[4]   H. Taniguchi, "Flexible Artificial Muscle Actuator Using Coiled Shape Memory Alloy Wires", Proc. the 3rd International Conference on Biomedical Engineering and Technology - ICBET , Copenhagen, Denmark, Vol. 7, pp. 54-59, May, 2013

[5]   M. Grebenstein, P. Van der Smagt, "Antagonism for a Highly Anthropomorphic Hand–Arm System", *Advanced Robotics*, Vol 22, No. 1, pp. 39-55, 2008

[6]   Y. Ariga, H. Pham, M. Uemura, H. Hirai, F. Miyazaki, "Novel Equilibrium-Point Control of Agonist-Antagonist System with Pneumatic Artificial Muscles", Proc. of the IEEE International Conference on Robotics and Automation, Minnesota, USA, pp. 1470-1759, 2012

[7]   Y. Nakanishi, S. Ohta, T. Shirai, Y. Asano, T. Kozuki, Y. Kakehashi, H. Mizoguchi, T. Kurotobi, Y. Motegi, K. Sasabuchi, J. Urata, K. Okada, I. Mizuuchi, M. Inaba, "Design Approach of Biologically-Inspired Musculoskeletal Humanoids", *International Journal of Advanced Robotics Systems*, Vol. 10, No. 216, pp 1-13, 2013

[8]   http://www.medicalnewstoday.com/articles/288012.php

[9]   A. Rodić, B. Miloradović, Đ. Urukalo, "Towards Building Of Lightweight Robot Arm Of Anthropomorphic Characteristics", International Conference On Electrical, Electronic And Computing Engineering-IcETRAN 2014, Vranjačka Banja, Srbija, 2-5.07.2014

[10]   Karanović V, Jocanović M, Jovanović V; "Review of Development Stages in the Conceptual Design of an Electro-Hydrostatic Actuator for Robotics", Acta Polytechnica Hungarica, Vol. 11, No. 5, pp. 59-79, 2014

[11]   Torani F, Farahmandzad H, Aghamirsalim M; "Gray-Box Modeling of a Pneumatic Servo-Valve", Acta Polytechnica Hungarica, Vol. 7, No. 5, pp. 129-142, 2010

[12]   https://en.wikipedia.org/wiki/Sagittal_plane#/media/File:BodyPlanes.jpg

[13]   D. Popov, I. Gaponov, J.-H. Ryu, "Bidirectional Elbow Exoskeleton Based on Twisted-String Actuators", *IEEE/RSJ International Conference on Intelligent Robots and Systems (IROS)*, pp. 5853,5858, 3-7 Nov. 2013

[14]   M. Suzuki, T. Mayahara, A. Ishizaka, "Redundant Muscle Coordination of a Multi-DOF Robot Joint by Online Optimization," *IEEE/ASME international conference on Advanced intelligent mechatronics,* pp. 1,6, 4-7 Sept. 2007

[15]   Maxon DC Motor, Re25, Graphite Brushes, 20W. Available data on the internet: http://www.maxonmotor.com/maxon/view/product/motor/dcmotor/re/re25/339150

[16] Maxon Planetary Gearhead GP 26A, 19.2:1, Available data on the internet: http://www.maxonmotor.com/maxon/view/product/gear/planetary/gp26/40 6762

[17] Maxon Encoder MR, CPT 1000. Available data on the internet: http://www.maxonmotor.com/maxon/view/product/sensor/encoder/Encoder -MR-TypML-128-1000imp-3Kanal/225780

[18] Axial bearing FAG 51100, Available data on the internet: http://www.fagbearing.com.cn/FAGbearinglist/FAG/FAG-51100.html

[19] ESCON Module, Servo controller. Available data on internet: http://www.maxonmotor.com/maxon/view/product/control/4-Q-Servokontroller/438725.

[20] LabView system design software. Available data on the internet: http://www.ni.com/labview/

[21] NI Single-Board RIO. Available data on the internet: http://www.ni.com/singleboard/

[22] N. Mohan, "Electrical Drives: An Integrative Approach", MNPERE, USA, ISBN 0-9715292-1-3

[23] T. Würtz, C. May, B. Holz, C. Natale, G. Palli, C. Melchiorri, "The Twisted String Actuation System: Modeling and Control," *Advanced Intelligent Mechatronics (AIM), 2010 IEEE/ASME International Conference on* , vol., no., pp. 1215,1220, 6-9 July 2010

[24] J. J. Guzek, C. Petersen, S. Constantin and H. Lipson, "Mini Twist: A Study of Long-Range Linear Drive by String Twisting", ASME. *J. Mechanisms Robotics.* 2012; 4(1):014501-014501-7

[25] M. Suzuki, "Complex and Flexible Robot Motions by Strand-Muscle Actuators, Climbing and Walking Robots: towards New Applications", Houxiang Zhang (Ed.), ISBN: 978-3-902613-16-5, InTech, 2007

[26] I.-W. Park; V. SunSpiral, "Impedance Controlled Twisted String Actuators for Tensegrity Robots," *14th International Conference on Control, Automation and Systems (ICCAS),* pp. 1331-1338, 22-25 Oct. 2014

[27] K. Levenberg, "A Method for the Solution of Certain Problems in Least Squares," *Quart. Appl. Math*. Vol. 2, pp. 164-168, 1944

[28] D. Marquardt, "An Algorithm for Least-Squares Estimation of Nonlinear Parameters," *SIAM J. Appl. Math*. Vol. 11, pp. 431-441, 1963